

Chapter 3

Kinetic Studies on the Initiation Mechanism of Olefin Metathesis

Catalysts with Chelating Alkylidenes

Kinetic Studies on the Initiation Mechanism of Olefin Metathesis Catalysts with Chelating Alkylidenes

Introduction

The study of mechanism has been critical to the development of olefin metathesis as a useful chemical transformation. Following the discovery of the olefin metathesis reaction, the ill-defined catalyst mixtures made it difficult to observe intermediates on the pathway and many different mechanisms were proposed.¹ The majority of these were “pairwise” mechanisms that involved metal complexes with two olefins bound at the same time (Figure 3.1). One of the most popular proposals invoked a coupling of the olefins to form a cyclobutane π -complex and cycloreversion to generate two new olefins.² This was by no means the only alternative; others included tetramethylene³ or metallacyclic intermediates.⁴

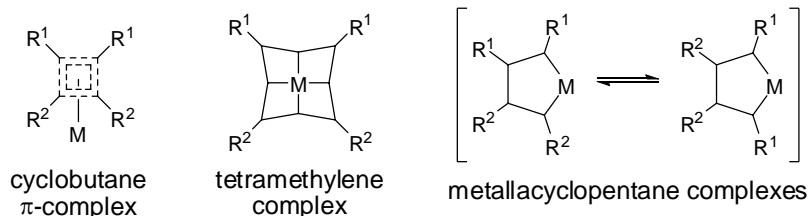


Figure 3.1. Proposed intermediates in “pairwise” mechanisms.

In the 1970s, Chauvin conducted several experiments whose results were difficult to rationalize based on a pairwise mechanism. Specifically, he found that ring-closing reactions with unsymmetrically substituted olefins gave mixtures of products instead of a single predicted product. This and other observations led him to propose the “non-pairwise mechanism” that is currently accepted today (Figure 3.2).⁵ The key intermediate in this mechanism is a metal alkylidene that at the time had not been observed in olefin metathesis reactions. The metal alkylidene binds olefin and undergoes cycloaddition to give a metallacyclobutane. Cycloreversion in the opposite direction gives a new metal alkylidene and a metal-coordinated olefin that can dissociate. Repeating this sequence can regenerate the starting alkylidene in the catalytic cycle. The crucial difference between this mechanism and the others was the sequential, rather than concurrent, interaction of olefins with the metal center.

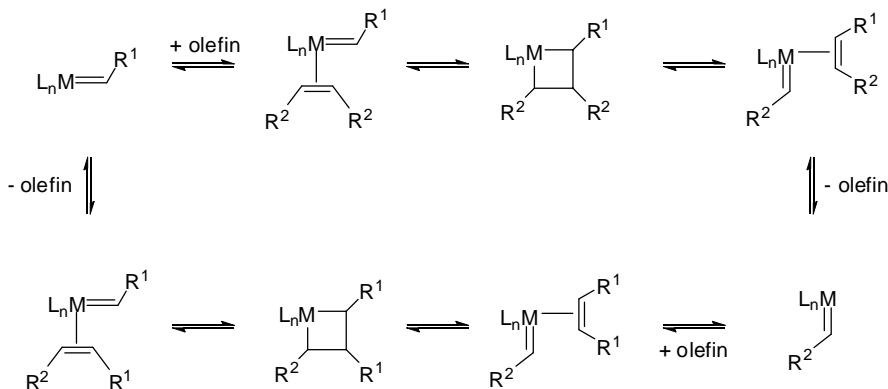


Figure 3.2. “Non-pairwise” mechanism for olefin metathesis.

The discovery of well-defined metal alkylidene species that were capable of catalyzing olefin metathesis gave a great deal of support to Chauvin’s proposed mechanism. Among the first examples of discrete complexes that produced catalytically active species was Tebbe’s reagent⁶ that allowed access to titanocenemethylidene **3.1** (Chart 3.1).⁷ This methylidene reacted with olefins to give metallacyclobutanes such as **3.2** that would catalyze metathesis. Schrock has also developed a family of metathesis catalysts based on molybdenum and tungsten alkylidenes, such as **3.3**, and studied catalytic olefin metathesis and the formation of metallacyclobutanes with these complexes.⁸

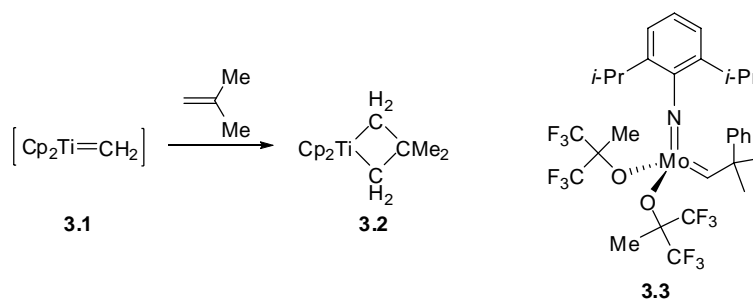


Chart 3.1. Early Transition Metal Alkylidenes and Metallacyclobutanes

The development of well-defined, late metal catalysts began with the synthesis of active ruthenium alkylidenes in the 1990s as described in Chapter 1.⁹ Subsequent mechanistic work has focused on characterizing the discrete steps in the olefin metathesis pathway catalyzed by complexes like **3.4** and **3.5**.¹⁰ These studies have been complicated by the fact that, until recently, intermediates on the reaction path have been difficult to observe.

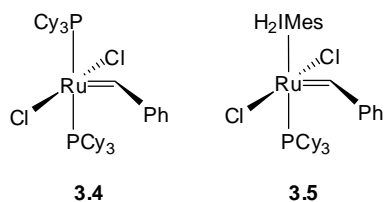


Chart 3.2. Common Ruthenium Metathesis Catalysts

The most well-studied portion of the catalytic cycle for ruthenium-based catalysts has been the initiation step,¹¹ since this is the most easily monitored. Early studies showed that the rate of catalysis was inhibited by the addition of phosphine, which suggests that, in the rate-determining step, phosphine loss is required for metathesis activity; however, this could be before or after olefin binding.¹² At first glance, the five-coordinate, 16-electron ruthenium alkylidene might be expected to react via an associative mechanism where olefin coordinates directly to the precatalyst (Pathway A, Figure 3.3). The alternative, loss of a phosphine to give a 14-electron intermediate that subsequently binds olefin, seems a less attractive possibility.

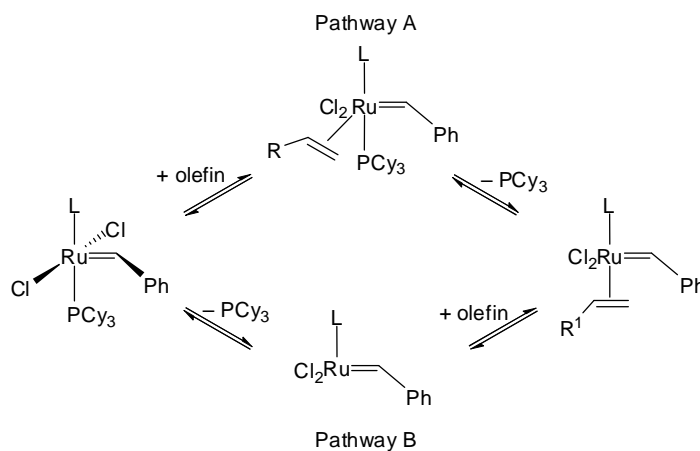


Figure 3.3. Mechanistic pathways differentiated by order of olefin coordination / phosphine loss.

A series of elegant mechanistic studies demonstrated that phosphine dissociation was the first step in the mechanism (Pathway B, Figure 3.3).^{13,14} Degenerate phosphine exchange in the absence of olefin was studied and a dissociative process established. An upper limit on the rate of phosphine dissociation could be defined, and subsequent reactions that probed the rate of a single metathesis event found that this rate was virtually identical to the rate of phosphine exchange. Additionally the rate of initiation was independent of the nature of the incoming olefin.

Together these observations led to the conclusion that olefin binding occurs only after phosphine dissociation. The overall mechanism for a degenerate metathesis reaction is shown in Figure 3.4.

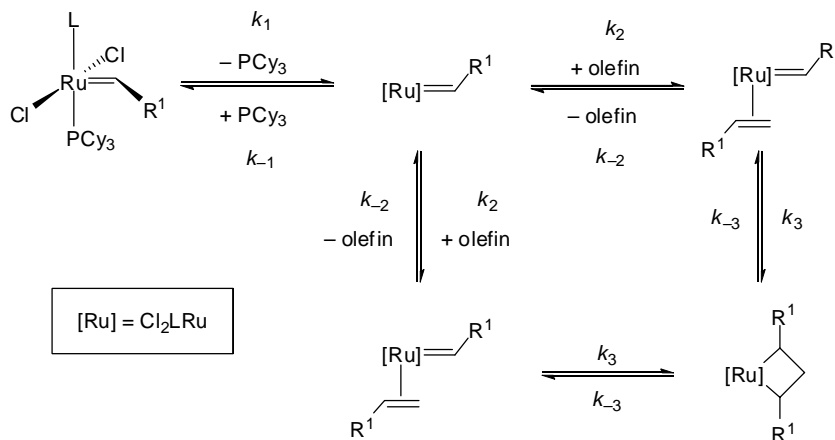


Figure 3.4. Representative mechanism for degenerate metathesis with phosphine catalyst.

A great surprise came when comparing the first-generation catalyst **3.4** with the second-generation catalyst **3.5**. Replacing a single phosphine ligand in **3.4** with the NHC ligand, H_2IMes , resulted in a 10^2 – 10^3 fold increase in catalyst activity for catalyst **3.5**. This increase was originally attributed to the NHC accelerating phosphine dissociation. However, when the degenerate phosphine exchange rates were measured, **3.5** was found to dissociate phosphine 100 times slower than **3.4**. Using a large excess of both phosphine and olefin the relative rates of olefin binding vs phosphine rebinding (k_2/k_{-1}) could be measured. In this case, it was found that the NHC complex was much more likely to bind olefin than the phosphine complex ($k_2/k_{-1} \sim 10^4$ greater) and this was the source of the higher activity.

While studying these reactions could rationalize the differences in catalyst activity, several aspects of the mechanism remain unclear. The initial olefin binding geometry, whether cis to the NHC (side-bound) or trans to the NHC (bottom-bound) remains a question. Several closely related models of bound olefin complexes have been prepared (Chart 3.3).¹⁵ Unfortunately these systems show examples for binding both trans (**3.6**) and cis (**3.7**, **3.8**) to the NHC. A better understanding of the geometry of olefin coordination will be critical to the rational design of stereo- or enantioselective metathesis catalysts.

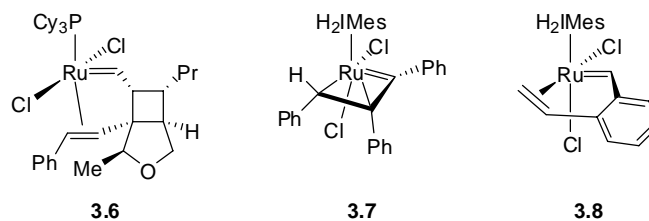
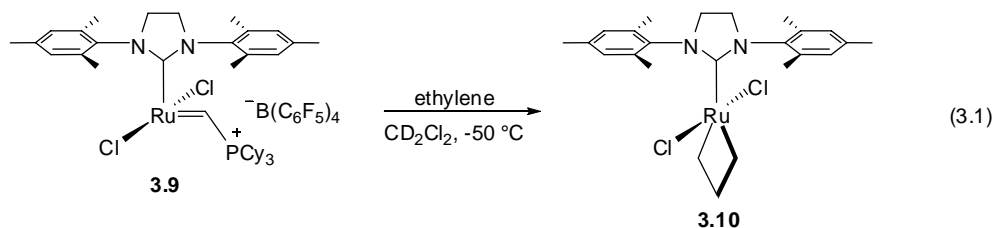


Chart 3.3. Olefin-Bound Model Complexes

The nature of the metallacyclobutane intermediates is also not completely understood. A great deal of our insight into these systems has been garnered from computational studies.¹⁶ Recently, by reacting the phosphonium alkylidene complex **3.9** with ethylene at low temperatures, a ruthenacyclobutane (**3.10**) that was stable at -40 °C could be characterized (eq 3.1).¹⁷ The lack of free PCy₃ that would stabilize ruthenium alkylidenes and the use of a four-coordinate precatalyst that did not require dissociation of a ligand for initiation allowed the formation of **3.10**. ¹H NMR studies of **3.10** established that the metallacycle is located trans to the NHC ligand. However, it is questionable whether this structure accurately reflects the geometry of olefin binding or assumes this geometry at a later stage.



Further NMR studies of this Ru cyclobutane showed that cycloreversion to the methyldiene–olefin complex and reformation of the metallacycle are very fast processes (I to II, Figure 3.5).¹⁸ Additionally, from structure II, rotation of the bound ethylene is fast relative to intermolecular olefin exchange. These results suggest that from the metallacycle, association of ethylene is the rate-limiting step in an intermolecular metathesis event.

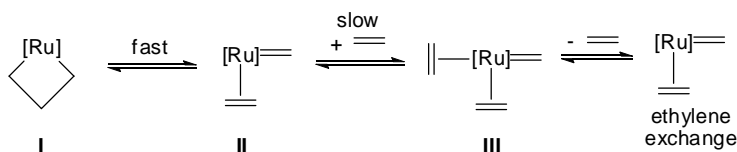


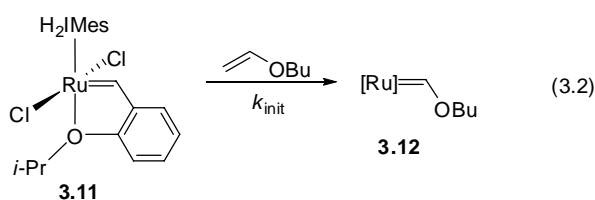
Figure 3.5. Olefin association and exchange from Ru metallacycle.

As the use of metathesis catalysts with chelating ligands has become more prevalent, understanding the real nature of catalyst initiation with these species becomes important. In Chapter 2 a number of ruthenium catalysts with chelating alkylidenes were shown to have quite different initiation behavior. By analogy to the phosphine case a “dissociative mechanism” has been proposed to understand the different behavior. This assumption has previously appeared in the literature,¹⁹ but no real experimental studies supporting this hypothesis have been conducted. In this work, the mechanism of initiation with chelated alkylidene complexes has been studied in an effort to better understand this process.

Results and Discussion

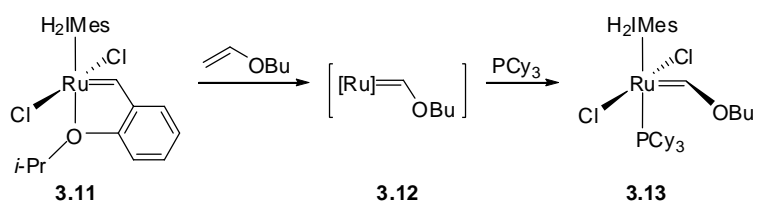
Beginning Studies of Initiation

The ether-containing catalyst **3.11** is the most commonly used chelated catalyst and was chosen as the starting point for mechanistic examinations.²⁰ Several challenges not faced when studying the initiation of phosphine-based catalysts such as **3.4** or **3.5** were important in this system. Degenerate phosphine exchange, which was so useful in elucidating the dissociative mechanism depicted in Figure 3.4, is clearly not applicable in these phosphine-free systems. Instead the primary tool has been reaction of **3.11** with substrates that form a catalytically inactive product. Directly functionalized olefins, such as vinyl ethers are good choices for this type of substrate as productive metathesis generates a Fischer carbene complex that is generally considered to be inert to further metathesis.²¹



Unlike the second-generation catalyst **3.5**, which reacts with vinyl ether to give a stable Fischer carbene complex directly, the phosphine-free catalyst **3.11** forms an unknown new complex. Upon reaction with *n*-butyl vinyl ether (BVE), the green color associated with **3.11** fades, yielding a pale yellow solution that is extremely air-sensitive (Scheme 3.1). In the ¹H NMR

spectrum, the benzylidene resonance of **3.11** is replaced by two new signals between 13 and 14 ppm (Figure 3.6). The new resonances are located in a region consistent with Fischer carbene complexes indicating productive metathesis has occurred. The definite identity of these complexes is still unknown, but the position and proportion of the two signals change based on temperature and olefin concentration, suggesting some sort of fluxional process. Possible structures include olefin- or oxygen-bound species or even a dimeric complex.²² Upon addition of excess PCy₃ an immediate color change to red occurs and both signals are replaced by a single resonance (13.94 ppm) corresponding to the known Fischer carbene complex **3.13**.



Scheme 3.1. Reaction of **3.11** with BVE

The kinetics of initiation of **3.11** by reaction with vinyl ether were conveniently studied using ¹H NMR spectroscopy. A large excess (> 15 eq) of BVE was used to ensure that the concentration of olefin did not change appreciably. The disappearance of the benzylidene resonance was monitored as a function of time and showed clean first-order kinetics. When the concentration of BVE was changed (0.080 M to 1.15 M) a first-order dependence on olefin was observed. This situation was very different than observed for the initiation of **3.5**, which was completely independent of olefin concentration. Using UV/Visible spectroscopy, the reaction could be tested with olefin concentrations as high as 2.5 M (30 wt. %, ~960 eq relative to [Ru]) with no evidence of saturation kinetics and an intercept very close to zero, again demonstrating the clean kinetics (Figure 3.7).

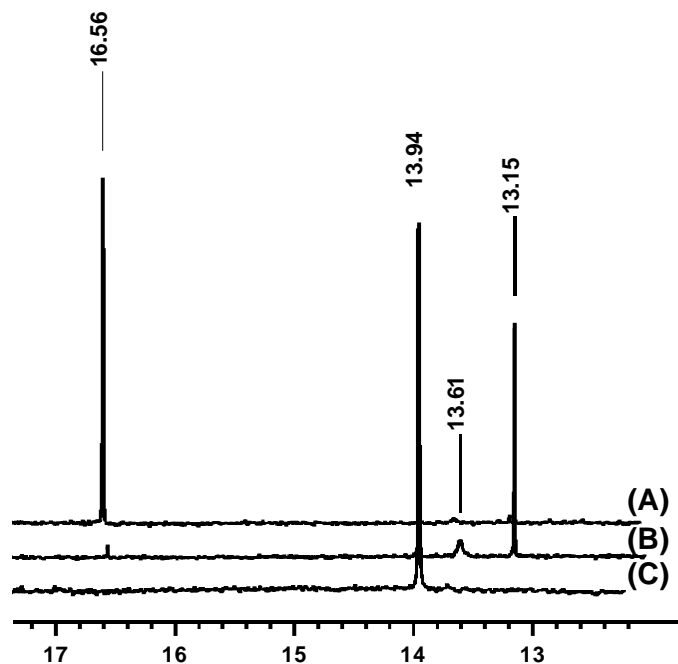


Figure 3.6. ^1H NMR spectra of reaction shown in Scheme 3.1 recorded in toluene- d_6 . (A) pure **3.11** (B) **3.11** reacted with 30 eq BVE (C) Reaction mixture following addition of PCy_3 .

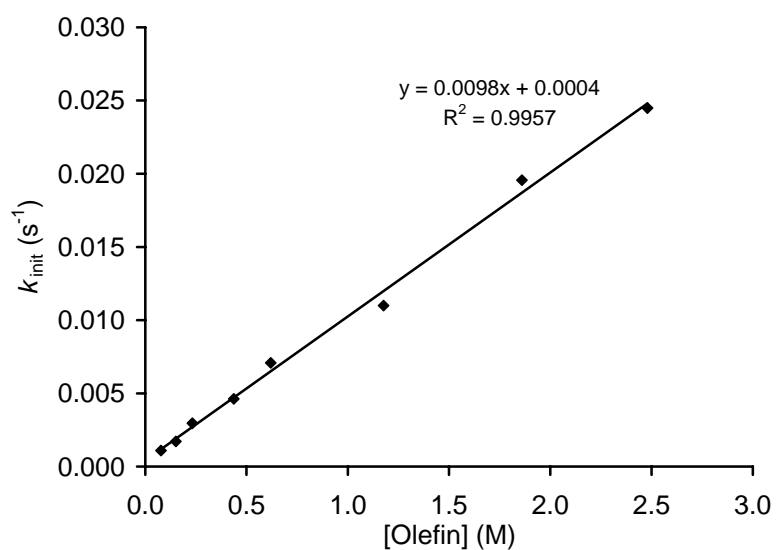


Figure 3.7. Plot of k_{init} versus [olefin] for catalyst **3.11**.

By measuring initiation rates at several temperatures (ranging from 0 °C to 30 °C) activation parameters could be extracted from an Eyring plot (see Experimental section). Values for ΔH^\ddagger of 15.2 ± 0.8 kcal/mol and ΔS^\ddagger of -19 ± 3 e.u. were obtained, which correspond to a ΔG^\ddagger of 20.69 ± 0.02 kcal/mol at 25 °C. These values are quite different than the activation parameters

for initiation of phosphine-based catalysts. For example the activation parameters reported for phosphine dissociation in **3.5**, which is rate determining, are $\Delta H^\ddagger = 27 \pm 2$ kcal/mol and $\Delta S^\ddagger = +13 \pm 6$ e.u., which correspond to a ΔG^\ddagger of 23.0 ± 0.4 kcal/mol. The most striking difference is the large and negative ΔS^\ddagger for **3.11**. Values more negative than -10 e.u. are generally indicative of an associative mechanism.²³ The phosphine-dissociation value of +13 e.u. conforms to the generally accepted dissociative mechanism. The enthalpies of activation are also quite different and are consistent with the associative olefin binding being the rate-determining step rather than breaking a Ru–P bond. For **3.11**, when the activation parameters are taken in conjunction with the first-order dependence on olefin, association of olefin seems to be the rate-determining step in catalyst initiation.

Two possibilities for the initiation mechanism are shown in Figure 3.8. Pathway A shows a “dissociative” mechanism, where the first step is a reversible dissociation of the donor ligand, L. This is followed by olefin binding, which is rate-limiting in this reaction. Pathway B depicts a more classical associative mechanism. In this case, the olefin binds to the ruthenium center and subsequent dissociation of the ligand L gives the olefin complex. This sort of mechanism was long considered more likely for catalysts such as **3.4**. Since the dissociating ligand L is linked to the catalyst and does not leave the coordination sphere before productive metathesis occurs, it is difficult to distinguish these mechanisms.

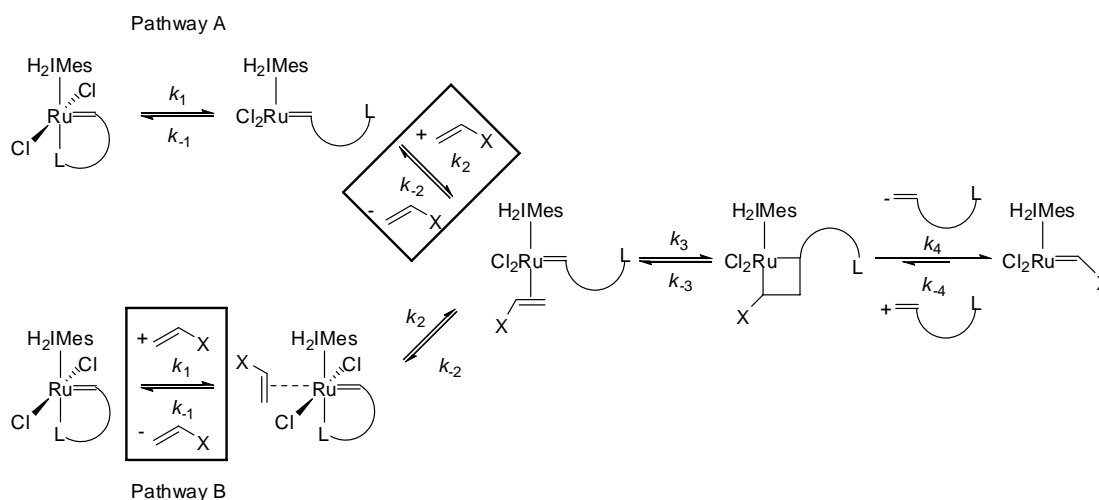


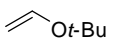
Figure 3.8. Mechanistic possibilities with olefin binding step highlighted.

Effect of Changes to Catalyst Structure and Incoming Olefin on Initiation

To further probe the mechanism of initiation, several effects were studied. These include varying the incoming olefin, changing the nature of the dissociating portion, altering the non-dissociating ligands on ruthenium, and moving to other systems. Additionally, solvent effects on the initiation kinetics were measured. All of these changes seemed to have a significant impact on initiation behavior.

With phosphine-based catalysts, the rate of initiation was generally independent of the incoming olefin.²⁴ This is not surprising given the operating dissociative mechanism. In the case of **3.11**, varying the incoming olefin resulted in major differences, all of which were consistent with an associative rate-determining step (Table 3.1). A series of olefins was chosen that would give complexes unlikely to undergo further reaction. BVE, *tert*-butyl vinyl ether, and ethyl vinyl sulfide all react to produce inactive Fischer carbene complexes. The unsaturated imine will form a catalyst described in Chapter 2 with negligible activity at room temperature.²⁵ Ethyl vinyl sulfide, the most electron-rich olefin, reacted the fastest with catalyst **3.11** at temperatures as low as -30 °C. The most sterically bulky olefin, *tert*-butyl vinyl ether, reacted the slowest. Again, only large and negative values of ΔS^\ddagger are observed; the larger ΔS^\ddagger for *tert*-butyl vinyl ether might result from more order in the transition state necessary to accommodate the bulky incoming olefin. The values of ΔH^\ddagger are also smaller for the more electron-rich olefins that can donate more electron density to the unsaturated ruthenium center.

Table 3.1. Initiation Kinetics for **3.11** With Different Incoming Olefins^a

| Catalyst | k_{init} (275 K) (10^{-4}s^{-1}) | ΔH^\ddagger (kcal/mol) | ΔS^\ddagger (e.u.) |
|---|---|-----------------------------------|----------------------------|
|  | 50 | 12.6 ± 0.8 | -25 ± 3 |
|  | 4.3 | 15.2 ± 0.8 | -19 ± 3 |
|  | 2.6 | 15.8 ± 1.5 | -18 ± 5 |
|  | 1.7^{b} | 12.3 ± 1.8 | -30 ± 4 |

^a Reactions were carried out in toluene-*d*₆, [Ru] = 5 mM, [olefin] = 0.15 M (30 eq).

^b Extrapolated from the Eyring plot.

While metathesis reactions can be carried out in a wide range of solvents, large effects on activity have been observed, particularly with coordinating solvents. For the initiation of **3.11**, the nature of the solvent seemed to have relatively little effect, even with coordinating THF (Table 3.2). Despite large differences in the dielectric constants of the various solvents no trend can be discerned. This contrasts with phosphine dissociation from **3.5** where increasing the solvent dielectric accelerated the rate of PCy₃ dissociation.

Table 3.2. Initiation Kinetics for **3.11** With Different Solvents^a

| Solvent | Dielectric Constant (ϵ) | k_{init} (275K) (10^{-4}s^{-1}) | ΔH^\ddagger (kcal/mol) | ΔS^\ddagger (e.u.) |
|---------------------------------|------------------------------------|---|--------------------------------|----------------------------|
| Toluene- <i>d</i> ₈ | 2.38 | 4.3 | 15.2 ± 0.8 | -19 ± 3 |
| THF- <i>d</i> ₈ | 7.32 | 3.0 | 14.1 ± 0.7 | -23 ± 3 |
| CD ₂ Cl ₂ | 8.97 | 4.0 | 13.7 ± 0.5 | -25 ± 2 |

^a Reactions were carried out with [Ru] = 5 mM, [olefin] = 0.15 M (30 eq).

Several changes to different aspects of the catalyst structure were made and evaluated (Chart 3.4). The results of the initiation reaction with BVE including rates at 275 K and the activation parameters are recorded in Table 3.3. The first modification was changing the oxygen substitution. Somewhat surprisingly, both methyl (**3.14**) and *tert*-butyl (**3.15**) ethers enhanced initiation relative to isopropyl substitution (**3.11**) (~4-fold increase in k_{init}). Two competing factors may be responsible for this result. From an electronic standpoint, the order of binding strength should be OMe < *Oi*-Pr < *Ot*-Bu based on increasing the donating ability of the alkyl group. From a steric standpoint, the order of binding should be *Ot*-Bu < *Oi*-Pr < OMe with the *tert*-butyl showing the most unfavorable interaction with the rest of the catalyst fragment and pushing off the ether. In composite, these two effects seem to counteract each other and the *Oi*-Pr substituent is poised to balance these two factors. The difference in initiation is reflected in the catalytic performance in RCM. When tested in the RCM of diethyl diallylmalonate (**3.19**) under standard conditions,²⁶ (eq 3.3) both **3.14** and **3.15** show modest improvements over **3.11** in catalytic performance, likely due to enhanced initiation (see Experimental section).

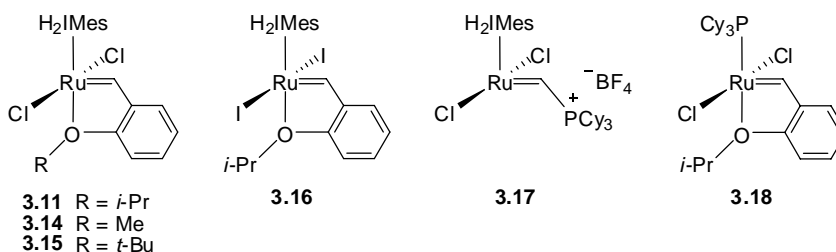


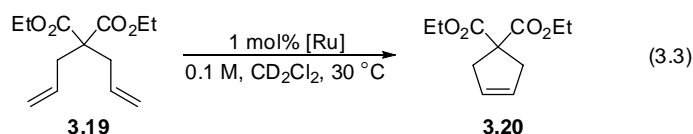
Chart 3.4. Different Catalysts Studied for Initiation

Table 3.3. Initiation Kinetics for Different Catalysts with BVE^a

| Catalyst | k_{init} (275 K) (10^{-4} s^{-1}) | ΔH^\ddagger (kcal/mol) | ΔS^\ddagger (e.u.) |
|-------------|---|--------------------------------|----------------------------|
| 3.11 | 4.3 | 15.2 ± 0.8 | -19 ± 3 |
| 3.14 | 19 | 12.6 ± 0.8 | -25 ± 3 |
| 3.15 | 14 | 14.6 ± 1.2 | -18 ± 5 |
| 3.16 | 0.15^{b} | 13.9 ± 1.3 | -30 ± 4 |
| 3.17 | 14^{b} | 9.0 ± 0.5 | -39 ± 2 |
| 3.18 | 0.046^{b} | 13.5 ± 0.7 | -34 ± 2 |

^a Reactions were carried out in toluene-*d*₆, [Ru] = 5 mM, [olefin] = 0.15 M (30 eq).

^b Extrapolated from the Eyring plot. ^c Reaction carried out in CD₂Cl₂.



Another modification in catalyst structure was to replace the chloride ligands with iodide. In the case of **3.5**, this modification gave a catalyst with increased phosphine dissociation (~200 times faster) but a smaller value for k_2/k_1 . This resulted in a iodide-substituted propagating species with similar activity. **3.16** was found to react with BVE significantly slower (~30-fold) than **3.11**. Size of the halides is the most likely explanation for this difference; larger iodide ligands can hinder either olefin association or a halide rearrangement necessary to bind olefin. When tested against **3.11** in the RCM of **3.19**, catalyst **3.16** shows lower activity and an induction period characteristic of inefficient catalyst initiation.

One of the most interesting comparisons for **3.11** is to a new class of four-coordinate ruthenium phosphonium alkylidenes recently reported by Romero and Piers.²⁷ Catalyst **3.17** requires no ligand dissociation in order to bind olefin.²⁸ Previously it has been observed that reaction of the similar **3.9** with 2-isopropoxystyrene was first-order in ruthenium and had

activation parameters suggestive of a bimolecular mechanism ($\Delta H^\ddagger = 8.6$ kcal/mol and $\Delta S^\ddagger = -41$ e.u.). The reaction of **3.17** with BVE showed similar activation parameters (Table 3.3). The low ΔH^\ddagger indicates that very little energy is required to facilitate olefin binding. The large, negative entropies of activation observed for all of the chelated catalysts compare well to the negative value for **3.17**. Given that this catalyst must work through a purely associative mechanism the similarity of these values argues for the olefin association following the ligand dissociation.

Catalyst **3.18** with a non-dissociating PCy₃ ligand was observed to initiate ~100 times slower than NHC-ligated **3.11**. Nevertheless, **3.18** also showed activation parameters consistent with an associative rate-determining step. This relationship is different than that between **3.4** and **3.5**, where **3.4** dissociated phosphine ~100 times faster than **3.5**. However, **3.4** was shown to have significantly lower propensity to bind olefin relative to phosphine. In the chelated variants, since the rate-limiting step involves the association of olefin, it is not surprising that first-generation systems are slower to initiate. These initiation rates do not necessarily reflect on the rates of oxygen dissociation. It may still be possible that oxygen dissociation is faster from **3.18** compared to **3.11**.

Changing the NHC for a phosphine has a major effect on the catalytic activity and initiation behavior. Exchanging one NHC for another also can have a great effect on this behavior (Chart 3.5). Catalyst **3.21** containing the bulky H₂IDIPP (H₂IDIPP = 1,3-bis(2,6-diisopropylphenyl)-4,5-dihydroimidazol-2-ylidene) ligand introduced by Mol has been shown to react very quickly with olefin substrates and give higher TONs than catalysts containing H₂IMes.²⁹ The corresponding ether-substituted catalyst (**3.22**) has received little attention.³⁰ The results of the RCM of **3.19** (eq 3.3) catalyzed by these systems are shown in Figure 3.9. From these data we can see that both H₂IDIPP variants catalyze metathesis faster than their H₂IMes analogs.

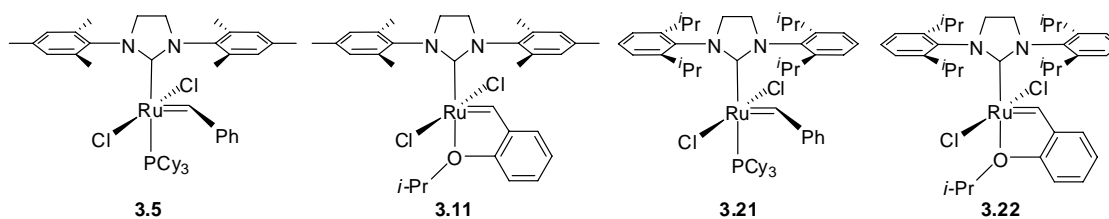


Chart 3.5. Catalysts Studied With a Bulky NHC Ligand

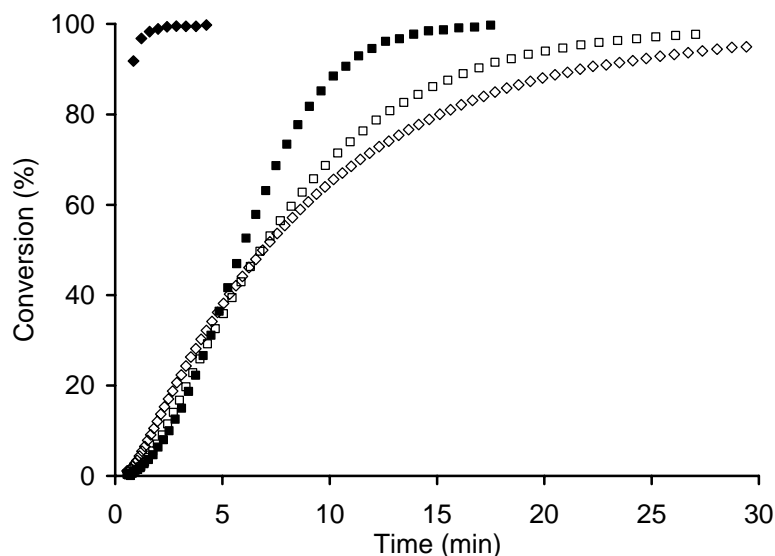


Figure 3.9. Conversion plot for RCM of **3.19** with **3.5** (\diamond), **3.11** (\square), **3.21** (\blacklozenge), and **3.22** (\blacksquare) (1.0 mol%, 30 °C, 0.1 M CD_2Cl_2).

The effect of the bulky H_2IDIPP ligand on the initiation behavior of both the phosphine-bound **3.21** and ether-coordinated **3.22** was tested and the results shown in Table 3.4. The bulky NHC greatly accelerates the phosphine dissociation and **3.21** was found to initiate ~360 times faster than **3.5**. These catalysts show similar large positive values for ΔS^\ddagger while **3.21** has a $\Delta H^\ddagger = 3$ kcal/mol lower than **3.5**. The bulky NHC ligand likely helps to push off the phosphine ligand reducing the value of ΔH^\ddagger . For the chelating ether complexes, **3.22** was found to initiate 20% slower than **3.11**, but both showed the characteristic bimolecular activation parameters. Despite its lower initiation rate, **3.22** still catalyzes the RCM of **3.19** more quickly than **3.11**. This must imply that the H_2IDIPP ligand is inherently more active than the H_2IMes ligand. In fact, for **3.22** the half-life for catalyst initiation with BVE is ~22 min, yet the reaction was complete in under 20

min. This suggests that only a small fraction of the catalyst is initiating, but these highly active fragments each catalyze many cycles.

The question remains as to why the initiation is slower with the chelating ether and a bulkier NHC. Two possibilities are shown in Figure 3.10 that differ based on whether or not the ether ligand dissociates prior to olefin coordination. If the olefin associates to the ether-bound

Table 3.4. Initiation Kinetics for Catalysts With a Bulky NHC Ligand^a

| Catalyst | k_{init} (303 K) (10^{-4}s^{-1}) | ΔH^\ddagger (kcal/mol) | ΔS^\ddagger (e.u.) | ΔG^\ddagger (303 K) (kcal/mol) |
|-------------|---|--------------------------------|----------------------------|---|
| 3.5 | 2.1 | 29.1 ± 0.6 | $+21 \pm 4$ | 22.95 ± 0.03 |
| 3.11 | 67 | 15.2 ± 0.8 | -19 ± 3 | 20.69 ± 0.02 |
| 3.21 | 720 ^b | 25.5 ± 1.4 | $+20 \pm 5$ | 19.4 ± 0.1 |
| 3.22 | 5.1 | 13.1 ± 0.3 | -31 ± 1 | 22.22 ± 0.01 |

^a Reactions were carried out with [Ru] = 5 mM, [olefin] = 0.15 M (30 eq). ^b Extrapolated from the Eyring plot.

complex then the bulkier NHC ligand can hinder olefin approach and binding (Case I). On the other hand, if the ether dissociates prior to olefin binding then rotation around the C–aryl bond may be necessary to move the free ether away from the olefin binding site. In this case, rotation will bring the *O*-*i*-Pr group closer to the NHC and the bulkier H₂IDIPP ligand should disfavor this process.

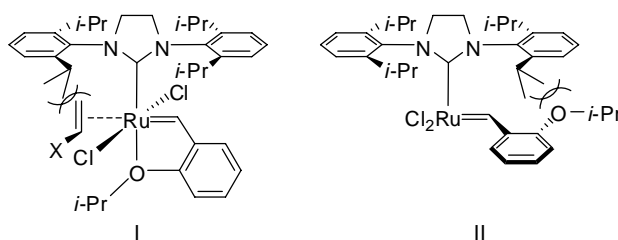


Figure 3.10. Possible sources of slower initiation with **3.22**.

Probing Initial Ligand Dissociation

To possibly determine whether olefin association precedes or follows dissociation of the O ligand, some method must distinguish these two steps. We decided that 2,6-substituted benzylidenes would be good candidates to study oxygen dissociation. This substitution will be particularly useful if an aryl rotation such as that shown in Figure 3.10 is necessary. In this event

The NHC-containing catalysts were tested in the initiation reaction with BVE and the same trend evident from the RCM studies was observed. The dimethoxy catalyst **3.25** initiated with BVE only at much higher temperatures (65 to 100 °C) than **3.14** and **3.26** (-25 to 0 °C), which only have one ether donor (Table 3.6). Similar activation parameters were observed for **3.14** and **3.26**, with moderate values for ΔH^\ddagger and ΔS^\ddagger . Complex **3.25** showed very different activation parameters, similar to phosphonium alkylidene **3.17**, with ΔH^\ddagger several kcal/mol lower and a very large negative ΔS^\ddagger . This large value for ΔS^\ddagger may reflect a significant ligand reorganization in the transition state. In fact, a different geometry may be required for **3.25** since a 180° bond rotation will not provide an open coordination site. This will case the catalytic species to have fewer degrees of freedom and result in larger negative entropies of activation.

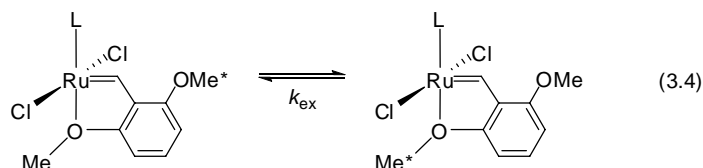
Table 3.6. Initiation Kinetics for 2,6-Substituted Benzylidene Catalysts ^a

| Catalyst | k_{init} (303 K) ^b (10 ⁻³ s ⁻¹) | ΔH^\ddagger (kcal/mol) | ΔS^\ddagger (e.u.) |
|-------------|---|--------------------------------|----------------------------|
| 3.14 | 7.7 ^c | 15 ± 1 | -19 ± 4 |
| 3.25 | .062 | 9 ± 2 | -47 ± 6 |
| 3.26 | 150 | 15 ± 2 | -13 ± 8 |

^a Reactions were carried out in TCE-*d*₂, [Ru] = 5 mM, [olefin] = 0.15 M (30 eq).

^b Extrapolated from the Eyring plot. ^c Reaction carried out in toluene-*d*₆.

Perhaps the most interesting aspect of the 2,6-dimethoxy substituted benzylidenes is the opportunity to study the exchange of the methyl groups (eq 3.4). ¹H-¹H EXSY spectra were recorded for **3.24** and **3.25** to test the possibility of observing exchange of the two methoxy groups. A representative spectrum is shown in Figure 3.11. The EXSY spectra showed exchange in **3.24** at room temperature but not in **3.25**. However at elevated temperatures, exchange of the methyl groups was observed for both complexes.



Quantitative rate data for the methoxy exchange could be obtained from line broadening experiments at elevated temperature. The rate of exchange was measured at several temperatures and activation parameters were determined (Table 3.7). From these data it is clear

that **3.24** does undergo methoxy group exchange faster than **3.25** despite its lower observed activity. This observation fits with the phosphine exchange data from **3.4** and **3.5** where the first-generation catalyst exchanges phosphine faster than the NHC variant but shows lower overall activity.

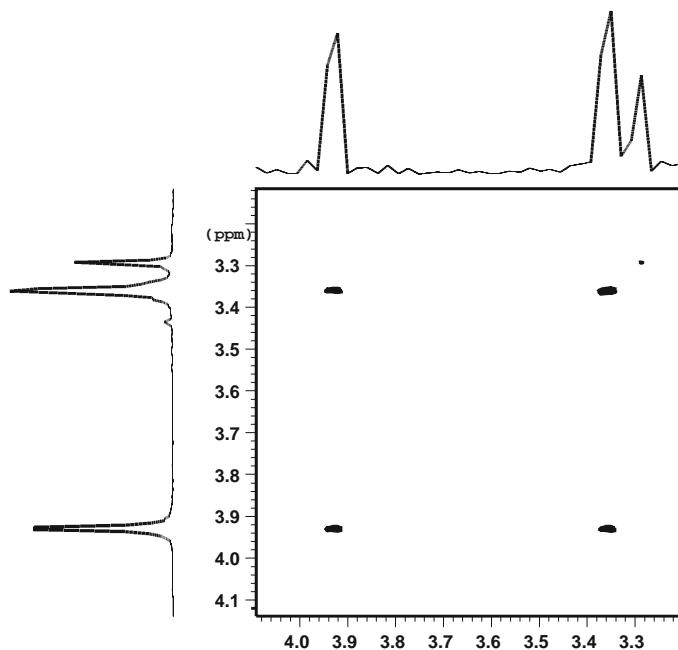


Figure 3.11. ^1H - ^1H EXSY spectrum showing exchange of methoxy groups in **3.24**.

Table 3.7. Methoxy Exchange Rates and Activation Barriers for **3.24** and **3.25**^a

| Catalyst | k_{ex} (368 K) (s^{-1}) | ΔH^\ddagger (kcal/mol) | ΔS^\ddagger (e.u.) | ΔG^\ddagger (368 K) (kcal/mol) |
|-------------|---|-----------------------------------|----------------------------|---|
| 3.24 | 42 | 20 ± 2 | $+ 4 \pm 5$ | 18.9 ± 2 |
| 3.25 | 4.2 | 20 ± 1 | $- 1 \pm 3$ | 20.7 ± 2 |

^a Exchange rates were determined from line broadening.

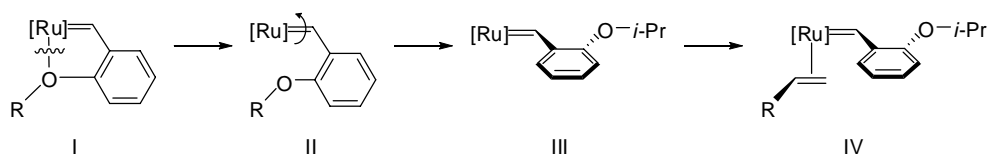
It is especially interesting to compare the rate of methoxy exchange in **3.25** with the initiation rate for the same catalyst (Table 3.8). At 95 °C the methoxy groups exchange ~3600 times faster than the catalyst initiates. It is probable that the methoxy groups do not exchange every time the ether dissociates, so the rate of O dissociation may be even higher. While this result still cannot absolutely distinguish whether olefin binding precedes or follows oxygen dissociation, it certainly demonstrates that in this system oxygen dissociation occurs much more quickly than olefin binding.

Table 3.8. Comparison of Exchange Rates and Initiation Rates for **3.25**

| Process | k_{obs} (s^{-1}) | Relative rate | ΔG^\ddagger (368 K) (kcal/mol) |
|--------------|--------------------------------------|---------------|--|
| OMe exchange | 4.4 | 3600 | 20.7 |
| Initiation | 0.0012 | 1 | 26.5 |

Summary of Mechanistic Data and Implications for Catalysis

Based on the mechanistic data, Figure 3.12 depicts our current picture of the initiation mechanism for catalyst **3.11**. This mechanism is similar to that observed for catalysts **3.4** and **3.5** where the first step is dissociation of the donor ligand to generate a 14-electron intermediate. This ether dissociation is fast and reversible and is accompanied by a rotation of the alkylidene and the C–aryl bond to position the ether away from the ruthenium and open as site for olefin binding. These rotational processes typically have very low energy barriers.³² The association of olefin is the rate-limiting step in this mechanism, while the remainder of the process occurs quickly.

**Figure 3.12.** Current picture of initiation mechanism for **3.11**.

The olefin coordination as the rate-determining step is well supported by the data. The first-order dependence on olefin concentration supports olefin involvement in the rate-limiting step and there was no evidence of changing the rate-determining step by increasing the concentration (up to 30 wt.%). The activation parameters measured for initiation with BVE are indicative of an associative mechanism. In particular, the large, negative value for ΔS^\ddagger reveals a bimolecular mechanism. Comparison to catalyst **3.17**, which clearly has rate-limiting olefin coordination, reveals very similar activation parameters. Finally, the dependence of initiation rate on the nature of the incoming olefin supports an associative mechanism where smaller, more electron-rich olefins react more quickly. All of these factors are markedly different than for catalysts **3.4** and **3.5** where phosphine dissociation is the rate limiting step.

The question of whether the ether dissociates prior to olefin coordination is more open. In many cases it is difficult to “prove” whether dissociation of a hemilabile ligand precedes or follows coordination of another reagent.³³ In this case, the most revealing observation was the rate of exchange of the two methoxy groups in **3.25**. This catalyst was found to exchange the two ethers ~3000 times faster than it would react with an external olefin. While this does not prove that olefin binds only when the ether is dissociated, it certainly demonstrates sufficient access to the 14-electron species that is a known catalytic intermediate. It seems unlikely that the incoming olefin would not react with this species. Also indicative of this type of intermediate is the fact that **3.16** and **3.18** initiate more slowly than **3.11**. Their 14-electron intermediates are known to have lower affinity for olefin than fragments with both NHC and chloride ligands and should initiate more slowly when olefin binding is rate-limiting.

By better understanding the mechanism by which these complexes react we can attempt to design more efficient catalysts. One important observation from this study is that, in general, chelating-ether catalysts initiate efficiently below room temperature. This is a result of the associative activation parameters, particularly the negative ΔS^\ddagger , giving more uniform initiation behavior across a wide temperature range. Their efficient initiation at low temperature supports the proposed “release–return” mechanism for **3.11** (Figure 3.13). The superior stability of this phosphine-free catalyst has been partially attributed to low amounts of active catalyst present at any time during the reaction. Although this catalyst initiates readily, the propagating species may also be trapped out during the reaction.

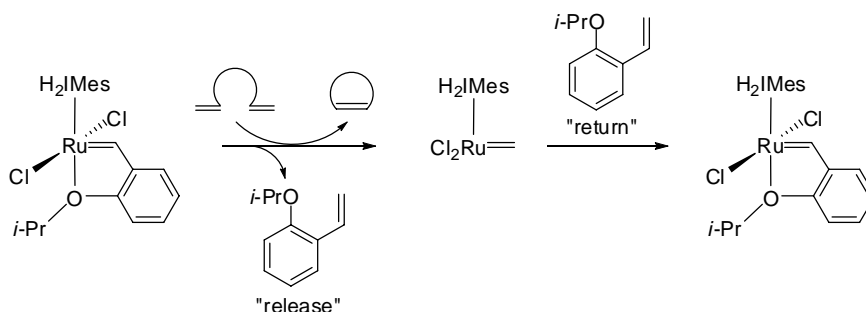
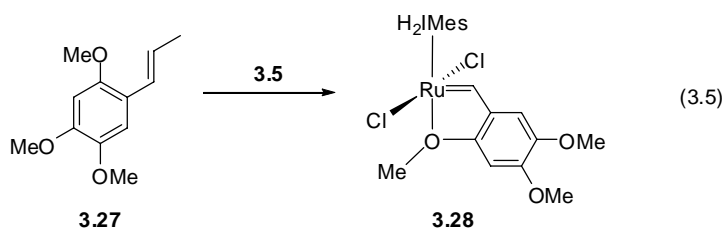
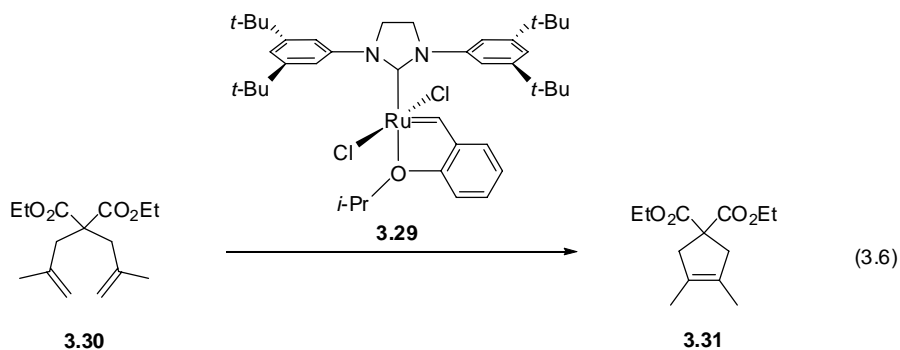


Figure 3.13. Release–return mechanism for **3.11**.

Relatively minor differences were observed when the oxygen substituent was varied. Though isopropyl has been the preferred substituent there is nothing “magical” about that group. With second-generation systems, the methyl ether initiates even more readily. In fact, **3.14** seems very similar to **3.11** in most applications (perhaps with a slightly lower stability). In many cases, methoxy-based catalysts could be a cost-effective alternative to isopropyl-substituted systems. Grela recognized this possibility and prepared a catalyst (**3.28**) that incorporates a benzylidene derived from α -asarone (**3.27**), a naturally occurring material (eq 3.5).³⁴



More demanding limitations on catalyst structure occur when modifying the non-dissociating portion. Most work on new catalyst development involves the replacement of H₂IMes with alternate ligands, including different NHCs.³⁵ Incorporation of bulky substituents on the NHC (such as replacing mesityl in **3.11** with 2,6-diisopropylphenyl in **3.22**) can hinder catalyst initiation. To further complicate matters, what may be considered less bulky from a reactivity standpoint may actually be more bulky for initiation purposes. For instance, catalyst **3.29** that has 3,5-di-*tert*-butylphenyl groups has been successfully applied in the RCM of **3.30** to form the tetrasubstituted olefin **3.31** (eq 3.6).³⁶ The increased reactivity toward hindered substrates was attributed to an open pocket formed by removing the ortho-substituents from the aryl rings. However, when tested in RCM to form the disubstituted olefin **3.20**, catalyst **3.29** showed a long induction period indicative of inefficient initiation. Presumably, the metal substituents interfere substantially with catalyst initiation.



Conclusions

The initiation mechanism for olefin metathesis catalysts with chelated alkylidenes has been studied in detail. Although it appears that dissociation of the ether portion in **3.11** occurs first, the rate limiting step is coordination of the incoming olefin. Beyond the initiation step the mechanism is still unclear. A deeper understanding of the initiation mechanism for this increasingly prevalent class of olefin metathesis catalysts should allow for more successful rational catalyst design, where the effects of changes in the catalyst framework can be predicted ahead of time.

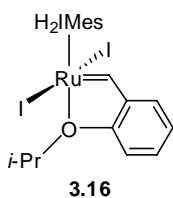
Experimental

Materials and Methods. All manipulations involving organometallic complexes (apart from chromatography) were performed using a combination of glovebox and Schlenk techniques under a nitrogen atmosphere. Unless otherwise indicated, all compounds were purchased from Aldrich, Alfa-Aesar, or Strem and used as received. Anhydrous solvents (purchased from Fisher) were rigorously degassed and obtained via elution through a solvent column drying system.³⁷ Deuterated solvents were purchased from Cambridge Isotope Laboratories, distilled from CaH₂ into a Schlenk tube, and degassed by freeze, pump, thaw cycles 3 times. Silica gel for the purification of organometallic complexes was obtained from TSI Scientific, Cambridge, MA (60 Å, pH 6.5–7.0). Catalysts **3.5**, **3.11**, **3.14**, **3.15**, **3.18**, **3.21**, and **3.22** were received as gifts from

Materia, Inc. **3.17** and $(\text{H}_2\text{IMes})(\text{py})_2\text{Cl}_2\text{Ru}=\text{CHPh}$ ³⁸ were prepared according to literature procedures. Diethyldiallyl malonate (**3.19**) was purchased from Aldrich and distilled before use.

Methods. NMR spectra were recorded on Varian Inova 500 and Mercury 300 spectrometers. ¹H NMR chemical shifts are reported in ppm relative to SiMe_4 ($\delta = 0$) and referenced internally with respect to the protio solvent impurity. ¹³C NMR spectra were referenced internally with respect to the solvent resonance. ³¹P NMR spectra were referenced using H_3PO_4 ($\delta = 0$) as an external standard. NMR reaction temperatures were determined by measuring the peak separations of an ethylene glycol or methanol standard.

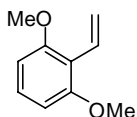
Synthesis of 3.16. In the drybox **3.11** (160 mg, 0.256 mmol) was dissolved in THF (5 mL) and



NaI (0.76 g, 5.1 mmol) was added in one portion. The mixture was heated to 65 °C for 3 h then cooled and the volatiles removed under vacuum. The residue was redissolved in CH_2Cl_2 and filtered through celite then concentrated to a green-brown residue. The residue was purified by column chromatography

(CH_2Cl_2 /pentane, 5% then 50%) and dried under vacuum to give catalyst **3.11** (148 mg; 0.182 mmol) as a green solid upon drying. Yield: 71%. ¹H NMR (CD_2Cl_2 , 300 MHz, δ): 15.67 (s, 1 H, $\text{Ru}=\text{CH}$), 7.59 (m, 1 H, Aryl H), 7.09 (s, 2 H, Mes), 7.01 (m, 1 H, Aryl H), 6.99 (s, 2 H, Mes), 6.87 (m, 2 H, Aryl H), 5.00 (sept., $J = 6.0$ Hz, 1 H, OCHMe_2), 4.12 (s, 4 H, $\text{NCH}_2\text{CH}_2\text{N}$), 2.65 (s, 6 H, Mes- CH_3), 2.50 (s, 6 H, Mes- CH_3), 2.44 (s, 3 H, Mes- CH_3), 2.33 (s, 3 H, Mes- CH_3), 1.40 (d, $J = 6.0$ Hz, 6 H, OCHMe_2).

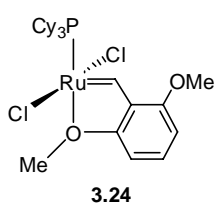
Synthesis of 2,6-dimethoxystyrene. Methyltriphenylphosphonium bromide (6.48 g, 18.1 mmol)



was suspended in THF (50 mL) and cooled to 0 °C. *n*-BuLi (1.6M in hexane, 8.5 mL, 13.6 mmol) was added to give a red-orange solution that was stirred for 1 h. 2,6-dimethoxybenzaldehyde (1.53 g, 9.18 mmol) was added and the solution immediately changed color to a milky white suspension that was stirred for 30 min warming to r.t. The reaction was quenched with acetone (2 mL) and poured into pentane (250 mL). The mixture was

filtered through celite and concentrated to an off-white solid that was purified by column chromatography (5% EtOAc/hexanes, $R_f = 0.32$) to give the product as a clear liquid. Yield: 0.73 g (48%). ^1H NMR (CDCl_3 , 300 MHz, δ): 7.17 (t, $J = 8.1$ Hz, 1 H, Aryl H), 6.99 (dd, $J = 18.0, 12.3$ Hz, 1 H, $\text{ArCH}=\text{CH}_2$), 6.57 (d, $J = 8.4$ Hz, 2 H, Aryl H), 6.08 (dd, $J = 18.0, 3.0$ Hz, 1 H, $\text{CH}=\text{CH}_2$), 5.46 (dd, $J = 12.0, 2.7$ Hz, 1 H, $\text{CH}=\text{CH}_2$), 3.85 (s, 6 H, ArOMe). $^{13}\text{C}\{^1\text{H}\}$ NMR (CDCl_3 , 75 MHz, δ): 158.75, 128.41, 127.51, 118.63, 115.05, 104.06, 55.88.

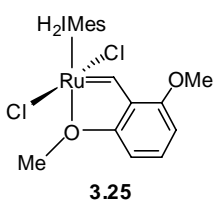
Synthesis of 3.24. In the drybox **3.4** (153 mg, 0.185 mmol) and CuCl (39 mg, 0.39 mmol) were



combined in C_6H_6 (5 mL). 2,6-dimethoxystyrene (60 mg, 0.36 mmol) was then added and the mixture heated to 60°C for 16 h. The volatiles were removed to a brown residue that was purified by column chromatography (Et_2O /pentane, 10% then 50%) and dried under vacuum to give catalyst **3.24**

(46 mg; 0.077 mmol) as a brown solid upon drying. Yield: 41%. ^1H NMR (CD_2Cl_2 , 300 MHz, δ): 17.64 (d, $J = 5.1$ Hz, 1 H, $\text{Ru}=\text{CH}$), 7.66 (t, $J = 8.4$ Hz, 1 H, Aryl H), 6.78 (d, $J = 8.4$ Hz, 1 H, Aryl H), 6.67 (d, $J = 8.4$ Hz, 1 H, Aryl H), 4.26 (s, 3 H, ArOMe), 3.95 (s, 3 H, ArOMe), 2.40–1.20 (m, 33 H, PCy_3). $^{31}\text{P}\{^1\text{H}\}$ NMR (CD_2Cl_2 , 121 MHz, δ): 61.80. HRMS–FAB (m/z): $[\text{M}]^+$ calcd for $\text{C}_{27}\text{H}_{43}\text{Cl}_2\text{O}_2\text{PRu}$, 602.1422; found, 602.1422.

Synthesis of 3.25. In the drybox **3.5** (150 mg, 0.177 mmol) and CuCl (39 mg, 0.39 mmol) were

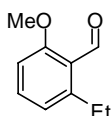


combined in CH_2Cl_2 (5 mL). 2,6-dimethoxystyrene (59 mg, 0.36 mmol) was then added and the mixture heated to 40°C for 16 h. The volatiles were removed under vacuum and the residue redissolved in CH_2Cl_2 (5 mL) and pentane (5 mL) then filtered through celite. The solution was concentrated to

a green-brown residue that was purified by column chromatography (Et_2O /pentane, 25% then 50%) and dried under vacuum to give catalyst **3.25** (93 mg; 0.15 mmol) as a green solid upon drying. Yield: 83%. ^1H NMR (CD_2Cl_2 , 300 MHz, δ): 17.24 (s, 1 H, $\text{Ru}=\text{CH}$), 7.56 (t, $J = 8.4$ Hz, 1 H, Aryl H), 7.08 (s, 4 H, Mes), 6.51 (d, $J = 8.1$ Hz, 1 H, Aryl H), 6.44 (d, $J = 8.4$ Hz, 1 H, Aryl H), 4.08 (s, 4 H, $\text{NCH}_2\text{CH}_2\text{N}$), 3.81 (s, 3 H, ArOMe), 3.73 (s, 3 H, ArOMe), 2.44 (s, 12 H, Mes-CH_3),

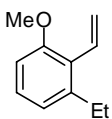
2.41 (s, 6 H, Mes-CH₃). ¹³C{¹H} NMR (CD₂Cl₂, 125 MHz, δ): 285.96 (Ru=CHAr), 211.23 (Ru-C(N)₂), 155.11, 147.49, 138.95, 138.87, 136.94, 131.76, 129.94, 128.83, 106.75, 104.78, 59.28, 56.23, 52.39, 21.57, 19.54. HRMS–FAB (m/z): [M]⁺ calcd for C₃₀H₃₆Cl₂N₂O₂Ru, 628.1198; found, 628.1198.

Synthesis of 2-ethyl-6-methoxybenzaldehyde. 6-ethylsalicylaldehyde (1.33 g, 8.88 mmol) and



K₂CO₃ (3.32 g, 24.0 mmol) were suspended in acetone (85 mL) and MeI (6.0 mL, 13.7 g, 96.3 mmol) was added via syringe. The mixture was heated to 60 °C for 16 h. The solvent was removed under vacuum and the residue dissolved in Et₂O (50 mL) and H₂O (50 mL). The layers were separated and the aqueous layer extracted with Et₂O (3 x 50 mL). The combined organics were washed with 2M NaOH, water, and brine then dried over MgSO₄. The solvent was concentrated to give a cloudy liquid that was purified by column chromatography (4% EtOAc/hexanes, R_f = 0.17) to give the product as a clear liquid. Yield: 1.20 g (82%). ¹H NMR (CDCl₃, 300 MHz, δ): 10.37 (s, 1 H, ArCHO), 7.69 (dd, *J* = 7.8, 1.8 Hz, 1 H, Aryl H), 7.47 (dd, *J* = 7.2, 1.8 Hz, 1 H, Aryl H), 7.06 (t, *J* = 7.8 Hz, 1 H, Aryl H), 3.89 (s, 3 H, ArOMe), 2.72 (q, *J* = 7.5 Hz, 2 H, ArCH₂CH₃), 1.26 (t, *J* = 7.5 Hz, 3 H, ArCH₂CH₃). ¹³C{¹H} NMR (CDCl₃, 75 MHz, δ): 190.53, 161.58, 138.52, 136.12, 129.42, 126.86, 124.76, 64.32, 22.29, 14.94.

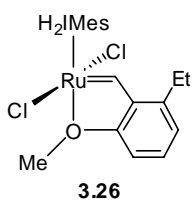
Synthesis of 2-ethyl-6-methoxystyrene. Methyltriphenylphosphonium bromide (4.84 g, 13.6



mmol) was suspended in THF (45 mL). *n*-BuLi (1.6M in hexane, 7.2 mL, 11.6 mmol) was added to give a red-orange solution that was stirred for 1 h. 2-ethyl-6-methoxybenzaldehyde (1.20 g, 7.29 mmol) was added and the solution immediately lightened to a yellow suspension that was stirred for 15 min. The reaction was quenched with acetone (2 mL) and poured into pentane (300 mL). The mixture was filtered through celite and concentrated to an off-white solid that was purified by column chromatography (5% EtOAc/hexanes, R_f = 0.32) to give the product as a clear liquid. Yield: 0.96 g (81%). ¹H NMR (CDCl₃, 300 MHz, δ): 7.38 (dd, *J* = 7.2, 1.8 Hz, 1 H, Aryl H), 7.15 (dd, *J* = 7.8, 1.8 Hz, 1 H, Aryl H), 7.06 (t, *J* = 7.5 Hz, 1 H, Aryl H), 7.04 (dd, *J* = 17.4, 10.8 Hz, 1 H, ArCH=CH₂), 5.74 (dd, *J* =

17.4, 1.2 Hz, 1 H, CH=CH₂), 5.31 (dd, *J* = 10.8, 1.2 Hz, 1 H, CH=CH₂), 3.75 (s, 3 H, ArOMe), 2.70 (q, *J* = 7.5 Hz, 2 H, ArCH₂CH₃), 1.25 (t, *J* = 7.5 Hz, 3 H, ArCH₂CH₃). ¹³C{¹H} NMR (CDCl₃, 75 MHz, δ): 155.97, 137.56, 132.10, 131.20, 129.15, 124.42, 124.25, 115.01, 61.71, 22.82, 15.21.

Synthesis of 3.26. In the glove box, a flask was charged with (H₂I₂Mes)(py)₂Cl₂Ru=CHPh (177



mg; 0.24 mmol), 2-ethyl-6-methoxystyrene (195 mg, 1.20 mmol), and toluene

(5 mL) and the reaction stirred at r.t. for 30 min. The volatiles were removed

under vacuum and the residue was washed with pentane (2 x 20 mL) to give a

brown solid. The solid was purified by column chromatography (Et₂O/pentane,

10% then 50%) and dried under vacuum to give catalyst **3.26** (21 mg; 0.033 mmol) as a green

solid upon drying. Yield: 14 %. ¹H NMR (CD₂Cl₂, 300 MHz, δ): 16.53 (s, 1 H, Ru=CH), 7.40 (d, *J*

= 7.2 Hz, 1 H, Aryl H), 7.07 (s, 4 H, Mes), 6.95 (t, *J* = 7.5 Hz, 1 H, Aryl H), 6.71 (d, *J* = 7.2 Hz, 1

H, Aryl H), 4.11 (s, 4 H, NCH₂CH₂N), 3.80 (s, 3 H, ArOMe), 2.79 (q, *J* = 7.5 Hz, 2 H, ArCH₂CH₃),

2.43 (s, 12 H, Mes-CH₃), 2.42 (s, 6 H, Mes-CH₃), 1.18 (t, *J* = 7.5 Hz, 3 H, ArCH₂CH₃).

Reaction of 3.11 with BVE, trapping with PCy₃. In the drybox, an NMR tube with a screwcap

septum was charged with **3.11** (5 mg) and CD₂Cl₂ (0.7 mL). Butyl vinyl ether (10 μL) was injected

and the reaction left at r.t. for 3 h. At this time the ¹H NMR showed two alkylidene resonances

located between 13 and 14 ppm. In the drybox PCy₃ (10 mg) was added to the NMR tube and

the color immediately changed from yellow to red. At this time the ¹H NMR showed a single

alkylidene resonance (13.94 ppm) corresponding to **3.13**.

NMR Initiation Kinetics. A stock solution was prepared to deliver the catalyst solution. Inside a

glovebox, a volumetric flask was charged with catalyst (0.024 mmol), and toluene-*d*₈ added to

prepare 2.0 mL of stock solution (0.012 M). An NMR tube with a screwcap septum top was

charged with catalyst stock solution (0.016 M, 0.25 mL, 3.0 μmol) and toluene-*d*₈ (0.035 mL).

The sample was equilibrated at the proper temperature in the NMR probe before the olefin (0.090

mmol, 30 eq, 0.15 M) was added via syringe. Reactions were monitored by measuring the peak heights of the starting alkylidene as a function of time over at least three half-lives.

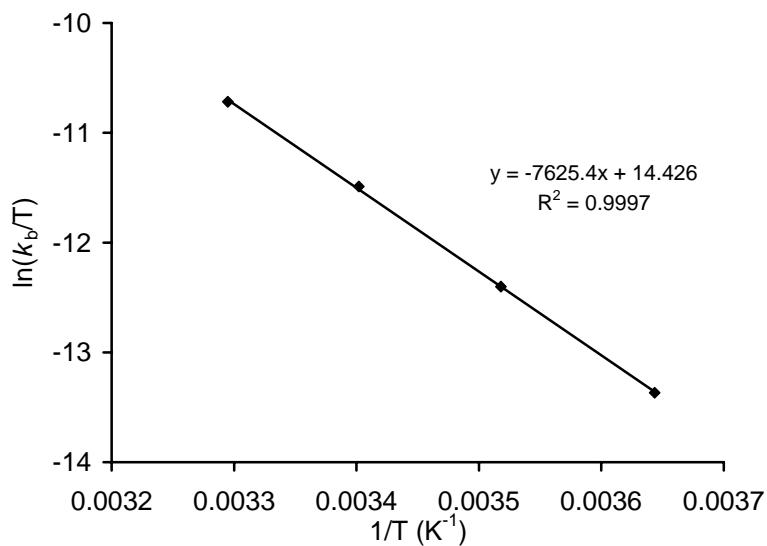


Figure 3.12. Eyring plot for reaction of **3.11** with BVE in toluene- d_8 from 0 °C–30 °C.

UV-Vis initiation kinetics. A stock solution was prepared to deliver the catalyst solution. Inside a glovebox, a volumetric flask was charged with catalyst (0.026 mmol) and toluene added to prepare 5.0 mL of stock solution (0.005 M). A cuvette fitted with a rubber septum was charged with catalyst stock solution (1.5 mL, 7.7 μmol) and toluene. The sample was equilibrated at 10 °C in the UV-vis spectrometer before BVE was added via syringe. The kinetics of the reaction were followed by monitoring the decrease in the peak at 585 nm.

RCM of 3.19 under standard conditions. A stock solution was prepared to deliver the catalyst solution. Inside a glovebox, a volumetric flask was charged with catalyst (0.016 mmol), and CD_2Cl_2 added to prepare 1.0 mL of stock solution (0.016 M). An NMR tube with a screwcap septum top was charged with catalyst stock solution (0.016 M, 50 μL , 0.80 μmol , 1.0 mol%) and CD_2Cl_2 (0.75 mL). The sample was equilibrated at 30 °C in the NMR probe before **3.19** (19.3 μL , 19.2 mg, 0.080 mmol, 0.1 M) was added via syringe. Data points were collected over an

appropriate period of time using the Varian array function. The conversion to **3.20** was determined by comparing the ratio of the integrals of the methylene protons in the starting material, δ 2.61 (dt), with those in the product, δ 2.98 (s).

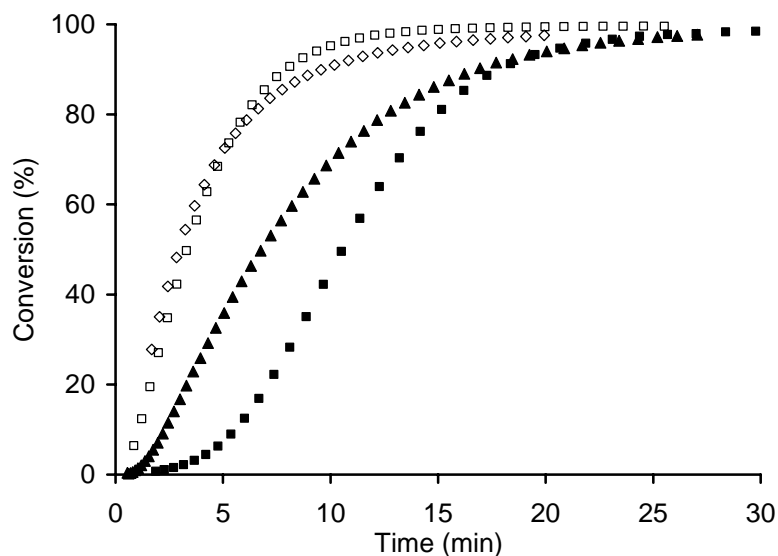


Figure 3.13. Conversion plot for RCM of **3.19** with **3.11** (▲), **3.14** (◇), **3.15** (□), and **3.16** (■) (1.0 mol%, 30 °C, 0.1 M CD₂Cl₂).

NMR Line Broadening Experiments. Variable temperature line shape data for catalysts **3.24** and **3.25** were recorded in 10-degree increments from the static spectrum (25 °C) until the temperature limit of the probe (120 °C) was reached. Line broadening of the bound and unbound methoxy groups was used to calculate first-order rate constants in the slow exchange region, according to eq 3.7.³⁹

$$k_{\text{obs}}^t = 1/\tau_t = \pi(w_t^{1/2} - w_0^{1/2}) \quad (3.7)$$

References and Notes

¹ Truett, W. L.; Johnson, D. R.; Robinson, I. M.; Montague, B. A. *J. Am. Chem. Soc.* **1960**, *82*, 2337–2340.

² Calderon, N.; Ofstead, E. A.; Ward, J. P.; Judy, W. A.; Scott, K. W. *J. Am. Chem. Soc.* **1968**, *90*, 4133–4140.

³ Lewandos, G. S.; Pettit, R. *Tetrahedron Lett.* **1971**, *12*, 789–793.

- ⁴ Grubbs, R. H.; Brunck, T. K. *J. Am. Chem. Soc.* **1972**, *94*, 2538–2540.
- ⁵ Hérisson, J.-L.; Chauvin, Y. *Makromol. Chem.* **1971**, *141*, 161–176.
- ⁶ Tebbe, F. N.; Parshall, G. W.; Reddy, G. S. *J. Am. Chem. Soc.* **1978**, *100*, 3611–3613.
- ⁷ Howard, T. R.; Lee, J. B.; Grubbs, R. H. *J. Am. Chem. Soc.* **1980**, *102*, 6876–6878.
- ⁸ Schrock, R. R.; Hoveyda, A. H. *Angew. Chem. Int. Ed.* **2003**, *42*, 4592–4633.
- ⁹ Trnka, T. M.; Grubbs, R. H. *Acc. Chem. Res.* **2001**, *34*, 18–29.
- ¹⁰ Sanford, M. S.; Love, J. A. Mechanism of Ruthenium-Catalyzed Olefin Metathesis Reactions. In *Handbook of Metathesis*; Grubbs, R. H., Ed.; Wiley-VCH: Weinheim, Germany, 2003; Vol. 1, pp 112–131.
- ¹¹ Initiation will be treated as the series of discrete steps in the first productive metathesis turnover.
- ¹² Dias, E. L.; Nguyen, S. T.; Grubbs, R. H. *J. Am. Chem. Soc.* **1997**, *119*, 3887–3897.
- ¹³ Sanford, M. S.; Ulman, M.; Grubbs, R. H. *J. Am. Chem. Soc.* **2001**, *123*, 749–750.
- ¹⁴ Sanford, M. S.; Love, J. A.; Grubbs, R. H. *J. Am. Chem. Soc.* **2001**, *123*, 6543–6554.
- ¹⁵ (a) Tallarico, J. A.; Bonitatebus, P. J., Jr.; Snapper, M. L. *J. Am. Chem. Soc.* **1997**, *119*, 7157–7158. (b) Trnka, T. M.; Day, M. W.; Grubbs, R. H. *Organometallics* **2001**, *20*, 3845–3847. (c) Anderson, D. R.; Hickstein, D. D.; O’Leary, D. J.; Grubbs, R. H. *J. Am. Chem. Soc.* **2006**, *128*, 8386–8387.
- ¹⁶ (a) Cavallo, L. *J. Am. Chem. Soc.* **2002**, *124*, 8965–8973. (b) Adlhart, C.; Chen, P. *J. Am. Chem. Soc.* **2004**, *126*, 3496–3510.
- ¹⁷ Romero, P. E.; Piers, W. E. *J. Am. Chem. Soc.* **2005**, *127*, 5032–5033.
- ¹⁸ (a) Wenzel, A. G.; Grubbs, R. H. *J. Am. Chem. Soc.* **2006**, *128*, 16048–16049. (b) Romero, P. E.; Piers, W. E. *J. Am. Chem. Soc.* **2007**, In Press.
- ¹⁹ Hoveyda, A. H.; Gillingham, D. G.; Van Veldhuizen, J. J.; Kataoka, O.; Garber, S. B.; Kingsbury, J. S.; Harrity, J. P. A. *Org. Biomol. Chem.* **2004**, *2*, 8–23.
- ²⁰ (a) Garber, S. B.; Kingsbury, J. S.; Gray, B. L.; Hoveyda, A. H. *J. Am. Chem. Soc.* **2000**, *122*, 8168–8179. (b) Gessler, S.; Randl, S.; Blechert, S. *Tetrahedron Lett.* **2000**, *41*, 9973–9976.
- ²¹ Louie, J.; Grubbs, R. H. *Organometallics* **2002**, *21*, 2153–2164.
- ²² Dias, E. L.; Grubbs, R. H. *Organometallics* **1998**, *17*, 2758–2767.
- ²³ Atwood, J. D. *Inorganic and Organometallic Reaction Mechanisms*; VCH: New York, 1997.
- ²⁴ Sanford, M.S. Ph.D. Thesis, California Institute of Technology, 2001.
- ²⁵ Hejl, A.; Day, M. W.; Grubbs, R. H. *Organometallics* **2006**, *25*, 6149–6154.
- ²⁶ Ritter, T.; Hejl, A.; Wenzel, A. G.; Funk, T. W.; Grubbs, R. H. *Organometallics* **2006**, *25*, 5740–5745.

- ²⁷ Romero, P. E.; Piers, W. E.; McDonald, R. *Angew. Chem. Int. Ed.* **2004**, *43*, 6161–6165.
- ²⁸ It has been proposed that alkylidene rotation necessarily precedes olefin binding for 3.17, see Romero, P. E. Ph.D. Thesis, University of Calgary, 2006.
- ²⁹ Dinger, M. B.; Mol, J. C. *Adv. Synth. Cat.* **2002**, *344*, 671–677.
- ³⁰ Courchay, F. C.; Sworen, J. C.; Wagener, K. B. *Macromolecules* **2003**, *36*, 8231–8239.
- ³¹ Maechling, S.; Zaja, M.; Blechert, S. *Adv. Synth. Catal.* **2005**, *347*, 1413–1422.
- ³² Straub, B. F. *Angew. Chem. Int. Ed.* **2005**, *44*, 5974–5978.
- ³³ Bassetti, M. *Eur. J. Inorg. Chem.* **2006**, 4473–4482.
- ³⁴ Grela, K.; Kim, M. *Eur. J. Inorg. Chem.* **2003**, 963–966.
- ³⁵ (a) Yun, J.; Marinez, E. R.; Grubbs, R. H. *Organometallics* **2004**, *23*, 4172–4173. (b) Despagnet-Ayoub, E.; Grubbs, R. H. *Organometallics* **2005**, *24*, 338–340. (c) Vehlow, K.; Maechling, S.; Blechert, S. *Organometallics* **2006**, *25*, 25–28. (d) Ledoux, N.; Allaert, B.; Pattyn, S.; Vander Mierde, H.; Vercaemst, C.; Verpoort, F. *Chem. Eur. J.* **2006**, *12*, 4654–4661.
- ³⁶ (a) Berlin, J. M. Ph.D. Thesis, California Institute of Technology, 2007. (b) Berlin, J. M.; Campbell, K.; Ritter, T.; Funk, T. W.; Chlenov, A.; Grubbs, R. H. *Org. Lett.* Submitted.
- ³⁷ Pangborn, A. B.; Giardello, M. A.; Grubbs, R. H.; Rosen, R. K.; Timmers, F. J. *Organometallics* **1996**, *15*, 1518–1520.
- ³⁸ Sanford, M. S.; Love, J. A.; Grubbs, R. H. *Organometallics* **2001**, *20*, 5314–5318.
- ³⁹ Günther, H. *NMR Spectroscopy, Second Edition*, John Wiley & Sons Limited: West Sussex, England, 1995, pp. 335–346.